

AFRL-AFOSR-UK-TR-2015-0002



Fatigue micromechanism characterization in carbon fibre reinforced polymers using synchrotron radiation computed tomography

**Serafina Consuelo Garcea
Prof S. Mark Spearing
Prof. Ian Sinclair**

**University of Southampton
University Road
Southampton, SO17 1BJ United Kingdom**

EOARD GRANT FA8655-11-1-3040

Report Date: December 2014

Final Report from 1 October 2011 to 30 September 2014

Distribution Statement A: Approved for public release distribution is unlimited.

**Air Force Research Laboratory
Air Force Office of Scientific Research
European Office of Aerospace Research and Development
Unit 4515, APO AE 09421-4515**

REPORT DOCUMENTATION PAGE

Form Approved OMB No. 0704-0188

Public reporting burden for this collection of information is estimated to average 1 hour per response, including the time for reviewing instructions, searching existing data sources, gathering and maintaining the data needed, and completing and reviewing the collection of information. Send comments regarding this burden estimate or any other aspect of this collection of information, including suggestions for reducing the burden, to Department of Defense, Washington Headquarters Services, Directorate for Information Operations and Reports (0704-0188), 1215 Jefferson Davis Highway, Suite 1204, Arlington, VA 22202-4302. Respondents should be aware that notwithstanding any other provision of law, no person shall be subject to any penalty for failing to comply with a collection of information if it does not display a currently valid OMB control number.
PLEASE DO NOT RETURN YOUR FORM TO THE ABOVE ADDRESS.

1. REPORT DATE (DD-MM-YYYY) 18 December 2014	2. REPORT TYPE Final Report	3. DATES COVERED (From – To) 1 October 2011 – 30 September 2014
--	---------------------------------------	---

4. TITLE AND SUBTITLE Fatigue micromechanism characterization in carbon fibre reinforced polymers using synchrotron radiation computed tomography	5a. CONTRACT NUMBER
	5b. GRANT NUMBER FA8655-11-1-3040
	5c. PROGRAM ELEMENT NUMBER 61102F

6. AUTHOR(S) Serafina Consuelo Garcea Prof S. Mark Spearing Prof. Ian Sinclair	5d. PROJECT NUMBER
	5d. TASK NUMBER
	5e. WORK UNIT NUMBER

7. PERFORMING ORGANIZATION NAME(S) AND ADDRESS(ES) University of Southampton University Road Southampton, SO17 1BJ United Kingdom	8. PERFORMING ORGANIZATION REPORT NUMBER N/A
--	--

9. SPONSORING/MONITORING AGENCY NAME(S) AND ADDRESS(ES) EOARD Unit 4515 APO AE 09421-4515	10. SPONSOR/MONITOR'S ACRONYM(S) AFRL/AFOSR/IOE (EOARD)
	11. SPONSOR/MONITOR'S REPORT NUMBER(S) AFRL-AFOSR-UK-TR-2015-0002

12. DISTRIBUTION/AVAILABILITY STATEMENT

Distribution A: Approved for public release; distribution is unlimited.

13. SUPPLEMENTARY NOTES

14. ABSTRACT
Carbon fiber reinforced polymers (CFRPs) are well established as an important weight-reducing structural technology, particularly within the aerospace sector due to their high specific stiffness and strength. CFRPs are widely identified as being very fatigue resistant, but typically this advantage is not fully exploited in design. Understanding and predicting the durability of these materials is of great interest. The current work aimed to delineate the micro-mechanisms of fatigue damage in carbon fiber-epoxy laminated composites using in situ and ex situ synchrotron radiation computed tomography (SRCT). Several novel observations have been obtained for the micro-mechanisms of fatigue crack growth. Broadly similar micro-mechanisms of damage initiation have been identified in fatigue and quasi-static loading in a particle-toughened carbon fiber-epoxy composite system. Results showed that damage propagation is closely related to the local microstructure. Toughened systems exhibit different damage behavior in resin-rich regions and fiber-packed zones, which appears to exaggerate non-uniform crack growth. Zones of retarded crack growth correspond to resin rich regions, which contain bridging ligaments. There is evidence that the load cycling contributes to progressive failure of bridging ligaments in the crack wake, especially in the toughened particle system. The un-toughened system showed more uniform damage propagation across the crack front, due to the more uniform microstructure and showed a higher number of fiber breaks within the 0° plies with respect to the toughened systems, particularly within regions close to the 0° ply splits. It seems likely that a key mechanism of fatigue in the toughened-particle system on intralaminar loading is the degradation of bridging ligaments introduced by particles in the fatigue crack wake rather than due to processes at, or ahead of the crack tip.

15. SUBJECT TERMS
EOARD, Composites, carbon fiber reinforced polymers, fatigue

16. SECURITY CLASSIFICATION OF:			17. LIMITATION OF ABSTRACT SAR	18. NUMBER OF PAGES 26	19a. NAME OF RESPONSIBLE PERSON Matt Snyder
a. REPORT UNCLAS	b. ABSTRACT UNCLAS	c. THIS PAGE UNCLAS			19b. TELEPHONE NUMBER (Include area code) +44 (0)1895 616420

Fatigue micromechanism characterisation in carbon fibre reinforced polymers using synchrotron radiation computed tomography

Serafina Consuelo Garcea

Supervised by
Prof. S. Mark Spearing
Prof. Ian Sinclair

AFOSR EOARD Program Monitor: Col. Randall Pollak

Engineering Materials Research Group
Faculty of Engineering and Environment
University of Southampton

December 2014

Table of Contents

Publications 3

Journal papers 3

Conference papers 3

1. Introduction 4

2. Materials and methodology 5

2.1 Material systems 5

2.2 Fatigue tests and SRCT scan procedure 6

2.3 Damage analysis 8

3. Damage initiation in particle toughened system 8

4. Effect of toughening strategies on fatigue micromechanisms 10

4.1 Particle toughened system 10

4.2 Untoughened system 12

4.3 Intrinsically toughened matrix system 13

4.4 Crack morphology 14

5. Fatigue damage quantification 16

6. Fatigue and quasi-static damage comparison 18

7. Conclusions 20

8. Significant Contributions 21

9. Future Work 22

Acknowledgments 22

References 23

Publications

This work has been disseminated through the following publications and conference presentations. AFOSR EOARD funding has been acknowledged in each publication and presentation:

Journal papers

- S.C. Garcea, M.N. Mavrogordato, A.E. Scott, I. Sinclair, S.M. Spearing, “Fatigue micromechanism characterisation in carbon fibre reinforced polymers using synchrotron radiation computed tomography”, *Composites Science and Technology*, Vol. 99, pp. 23-30, 2014.
- S.C. Garcea, I. Sinclair, S.M. Spearing, “*In situ* synchrotron tomographic evaluation of the effect of toughening strategies on fatigue micromechanisms in carbon fibre reinforced polymers”, submitted to *Composites Science and Technology*, in review.
- S.C. Garcea, I. Sinclair, S.M. Spearing, “Fatigue damage initiation in carbon fibre reinforced polymers using synchrotron radiation computed tomography”, journal letter, in preparation.
- S.C. Garcea, I. Sinclair, S.M. Spearing, “Size effect study of particle toughened carbon/epoxy under fatigue loading using high-resolution synchrotron radiation computed tomography imaging”, in preparation.

Conference papers

- S.C. Garcea, M.N. Mavrogordato, A.E. Scott, I. Sinclair, S.M. Spearing, “Synchrotron computed tomography of fatigue micromechanisms in CFRP”, *Proceeding of 19th International Conference on Composite Materials*, Montreal, 2013.
- S.C. Garcea, I. Sinclair, S.M. Spearing, “Characterisation of fatigue micromechanisms in toughened carbon fiber-polymer composites using synchrotron radiation computed tomography”, *Proceeding of the 16th European Conference on Composite Materials*, Seville, 2014.

1. Introduction

Carbon fibre reinforced polymers (CFRPs) are well established as an important weight-reducing structural technology, particularly within the aerospace sector due to their high specific stiffness and strength [1]. Whilst CFRPs are widely identified as being very fatigue resistant, typically this advantage is not fully exploited in design. As such, understanding and predicting the durability of these materials is of great interest. Fatigue design methodologies for composite laminates are not well-established due to degradation via multiple interacting damage modes, including fibre/matrix debonding, matrix cracking, delamination, and fibre breaks [2]. Previous studies have focused on assessing fatigue damage mechanisms and the link to fatigue life using various experimental techniques [2-8]. However, reliable predictions based on physical observations remain key to improving CFRP structural design. Different non-destructive techniques have been employed historically to detect fatigue damage in composites: for example, ultrasonic C-scans to evaluate delamination [9,10], acoustic emission to monitor the formation and growth of damage [11,12], thermography and thermo-elastic stress analysis to correlate damage and surface strains [13]. These methods have intrinsic limitations, such as the inability to provide direct information on type, size and orientation of damage, to resolve fine-scale failure events (*e.g.* fibre/matrix debonding and fibre breaks), and to provide a thorough three-dimensional representation of damage. In this respect, computed tomography (CT) has become established as a powerful technique for contemporary material science studies, allowing multiscale analysis (macro-, meso-, micro- and nano-scale) of material structure and damage to be performed [14]. Previous studies conducted on CFRPs have demonstrated that high resolution CT allows the imaging of damage at the scale of individual broken fibres [15], and that a voxel resolution on the order of one micrometre is reasonable to detect and distinguish fundamental damage modes [15-18].

The current work has the aim of delineating for the first time the micromechanisms of fatigue damage in carbon fibre-epoxy laminated composites using *in situ* and *ex situ* synchrotron radiation computed tomography (SRCT). The ability to explore three-dimensional volumes is of fundamental importance in multidirectional laminates that exhibit multiple damage mechanisms, as in this work. Performing *in situ* experiments is relevant to follow damage propagation, capturing the chronology of micro-

mechanistic interactions. Mechanically representative constraint conditions are preserved (triaxiality, residual stress states), whilst sectioning artefacts and relaxation processes associated with surface preparation are avoided. The objectives of this project have three elements: first to conduct an investigation of the mechanisms that underpin fatigue behaviour across a range of composite systems employing different toughening strategies. At this stage two- and three-dimensional damage imaging reveals similarities and differences associated with toughened and untoughened systems. The second element is to evaluate the micromechanisms of fatigue damage initiation in a particle-toughening system, assessing the role of toughening particle at the early stage of fatigue failure. The third element is the quantification of damage and the investigation of the effectiveness of toughening mechanisms in order to inform modelling.

2. Materials and methodology

2.1 Material systems

Three carbon/epoxy material systems, all produced by the Hexcel Corporation, have been assessed in the present work: two toughened systems; one containing thermoplastic toughening particles (T700/M21), the other utilizing a homogeneous, intrinsically toughened matrix (IM7/8852), and an untoughened system (IM7/3501-6). All systems contain intermediate modulus carbon fibres. A cross-ply lay-up was used, with a $[90/0]_8$ stacking sequence for the particle-toughened system, and a $[90/0]_{2s}$ lay-up for the other two systems. The nominal overall laminate thickness was maintained at ~ 1 mm for all three systems.

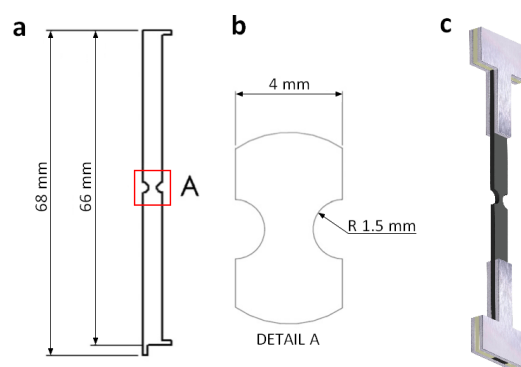


Figure 1- Coupons used: (a) geometry and dimensions of the specimen, (b) detail of the notch, and (c) specimen with tabs bonded.

Materials were laid up and auto-clave cured as flat plates using a standard aerospace cure cycle [19-21]. Rectangular coupons containing two semi-circular notches of radius 1.5 mm were introduced by water jet cutting, leaving a nominal central cross-section between the notches of 1 mm.

The geometry and the dimensions of the specimens used are shown in Figure 1. The coupon length was selected with the requirement to fit the specimen into the compact/portable fatigue-loading device to perform *ex situ* and *in situ* experiments, which resulted in lengths of 68 mm and 34 mm respectively. In addition, for the specimens used for *ex situ* scans, aluminium tabs were glued with the aim of loading them in the tensile rig. The average ultimate tensile failure strength (UTS) for each material system has been evaluated in previous studies [16], and is calculated based on the failure load and the net cross-sectional area between the notches. Values reported are: 918 MPa for the particle-toughened system, 1419 MPa for the untoughened, and 1271 MPa for the intrinsically toughened system [16].

2.2 Fatigue tests and SRCT scan procedure

Fatigue loading conditions and scan procedure were slightly different, depending on the specific objectives of the experiment. The experimental settings were divided into three sections for clarity.

Set 1 Damage initiation evaluation

The main aim of these experiments was to initiate damage in both fatigue and quasi-static cases. Therefore, the peak load considered was relatively low, 30% UTS for the fatigue case and 35% UTS for the quasi-static loading. Two hundred fatigue cycles were applied at a frequency of 5 Hz, with an R-ratio (maximum:minimum load) =0.1. Pre-fatigued coupons were loaded, using 90% of the load peak, in the *in situ* loading rig, to open the cracks initiated, but at the same time avoid any further propagation. Quasi-static experiments were conducted by loading the specimen *in situ* and holding at the peak load while imaging. A high voxel resolution of 0.325 μm was chosen in order to obtain the clearest possible indication of the earliest stages of damage. This is the first time that such a high CT resolution has been used to damage in composite materials.

Set 2 Assessment of the influence of toughening strategies

Fatigue cycling was initially carried out at a frequency of 5 Hz with a peak load of 50% UTS and $R=0.1$ using a standard servo-hydraulic load frame to apply 700 load cycles. After the pre-cycling had been applied, each specimen was placed in the *in situ* load frame, and a load just below the maximum peak load (~90% of peak) was applied to open the cracks, and the coupon was scanned. Following these initial scans, the *in situ* load frame was used to apply an additional 100 cycles, and then the specimens were imaged again. A voxel resolution of 0.69 μm was used. For the particular micromechanistic focus of this work, a balance between resolution and field of view was employed, allowing detailed observations to be made along the initial and propagated crack paths.

Set 3 Damage quantification

Tensile fatigue tests with a peak load of 30% and 50% of the nominal UTS were performed using a load ratio of $R=0.1$. Experiments were conducted at 10 Hz, up to a 10^4 cycles. The pre-fatigue coupons were loaded (~90% of peak) in the tensile loading rig during the scan to allow the opening of the crack. Quasi-static tests were conducted with the aim to create a similar crack length (split) to the fatigue case, allowing a direct comparison between the modes of crack extension. The required tensile loads were 60% UTS and 70% UTS, which are higher than those used for fatigue. The voxel resolution chosen was 1.5 μm , which again represents a trade-off between the resolution desirable and the optimum field of view (*i.e.* keeping the entire damage region inside the field of view). The voxel resolution used for the quasi-static tests was very similar, at 1.4 μm .

Scans were conducted at the Swiss Light Source (SLS), TOMCAT-X02DA Beamline, Paul Scherrer Institut, Switzerland. Beamtime was obtained via a competitive bidding process and peer evaluation. The specimens were placed at a distance of ~22-30 mm from the detector to allow a degree of phase contrast edge enhancement to be obtained (near-field Fresnel conditions). This facilitates the identification of cracks with small opening displacements. During each tomographic scan, 1500 projections were collected through the rotation of 180°. The beam energy was in the range of 14-

19 KeV. Three-dimensional reconstruction was obtained from radiographs using an in-house (SLS) code based on the GRIDREC/FFT approach [22].

2.3 Damage analysis

Micromechanical analysis of damage initiation and propagation has been conducted considering 2D slices. Damage segmentation allowed the 3D visualization of the different damage modes, their reciprocal location, and understanding the influence of microstructure on the crack growth, as shown in Figure 2. Segmentation was performed using the VG studio Max v2.1 package via a “seed-growing” algorithm.

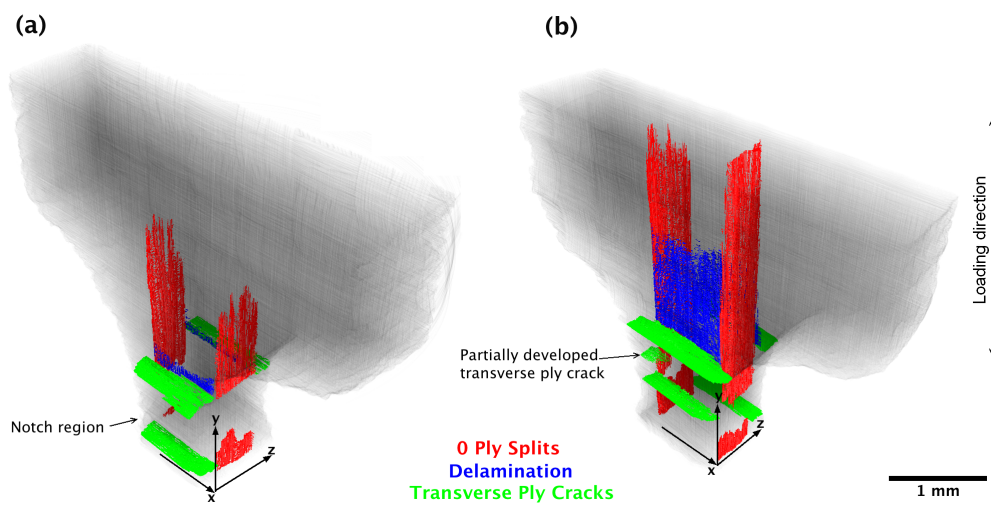


Figure 2 – Three-dimensional fatigue damage for: (a) 30% UTS and (b) 50% UTS, at 10^4 load cycles.

Segmented crack volumes were separately extracted and quantified in terms of crack length (considered as maximum extension), and Crack Opening Displacement (COD). Specifically, the public domain software, ImageJ was employed to binarize the crack volume, and basic image processing. The data obtained has been processed via MATLAB to describe the crack front shape and the COD corresponding to the root and near-tip regions of the 0° ply splits.

3. Damage initiation in particle toughened system

The results obtained from the fatigue tests showed that particles do not exhibit an active role in terms of 0° ply split initiation, and do not represent the location where damage occurs in the first instance. Cracks nucleate in the resin between fibres in the fibre-packed regions within the 0° plies (Figure 3(a)), and at this early stage do not

propagate into the resin rich regions. Damage is discontinuous: many parallel microcracks initiate, separated from each other by the presence of small bridging ligaments (on the order of a few micrometers), as is clearly visible in Figure 3(b). The small bridging ligaments detected along the fibre/matrix interface fail progressively due to cyclic loading, as shown in Figure 3(c) and 3(d), where the nucleation locations are indicated with white arrows. The bridging between them, as shown in Figure 3(b) is failed and the crack appears continuous. A direct comparison with the quasi-static case (Figure 3(e) and 3(f)), using a similar peak load, exhibits similar behaviour to the fatigue case (Figure 3(a) and 3(b)), *i.e.* locally discontinuous crack formation.

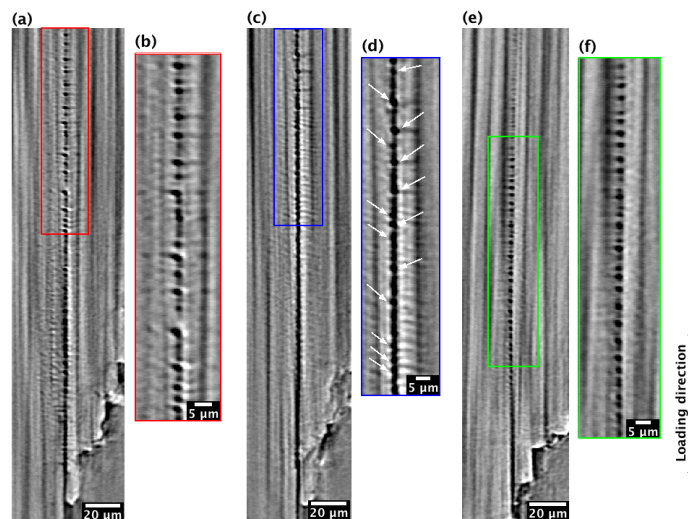


Figure 3 - Cross-sections parallel to the loading direction of 0° ply split: (a)-(b) discontinuous fatigue damage initiation for a peak load of 30% UTS and 200 cycles, (c)-(d) continuous fatigue damage for a peak load of 30% UTS and 200 cycles, (e)-(f) quasi-static case for a load of 35% UTS.

Three-dimensional rendering of the 0° ply splits for the fatigue and quasi-static case are reported in Figure 4. A somewhat longer crack length, larger number of crack initiation sites across the ply thickness, and longer single “spikes” characterize the fatigue case, as shown in Figure 4(a). In contrast, the quasi-static case shows damage mainly localized over only half of the ply thickness, with smaller and more frequent peaks, as shown in Figure 4(b). A noticeable difference between the two loading conditions is a reduction in the number density of bridging ligaments in the fatigue case, Figure 4(a).

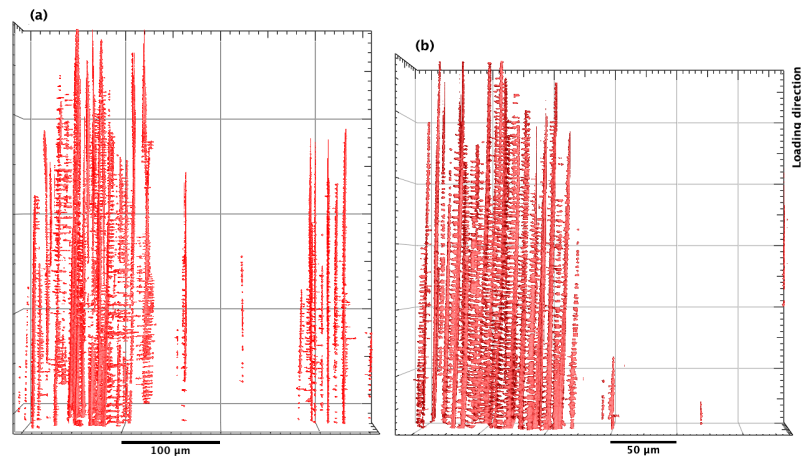


Figure 4 – Three-dimensional rendering of damage initiation in the fibre-packed regions: 0° ply split in (a) fatigue case with peak load of 30% UTS up to 200 cycles, (b) quasi-static case for a load of 35% UTS.

From these observations it appears that the initial stage of fatigue damage development consists of the nucleation of very localized cracks, which tend to grow parallel to the loading direction. Their coalescence across the ply thickness (perpendicular to the loading direction) is initially limited. The quasi-static case displays more apparent connections between initiation sites across the ply thickness (split width), and more bridging ligaments along the loading direction, as shown in Figure 4(b).

4. Effect of toughening strategies on fatigue micromechanisms

4.1 Particle toughened system

The particle-toughened M21/T700 system showed highly non-uniform growth of the fatigue crack front [23]. Detailed imaging has been focused on resin rich regions with the aim of understanding potential shielding mechanisms that may influence the overall damage progression, see Figure 5. Damage development appears very discontinuous in the resin rich regions, characterized by multiple microcracks, which are mainly associated with the debonding of toughening particles, as shown in Figure 5a. Interfacial debonding of particles tends to follow a specific direction: damage is typically oriented at 45° with respect to the loading direction, and this is consistent with the influence of macroscale shear on what appears to be essentially a tensile particle debonding/crack initiation process at the microscale. The growth of a 0° ply split associated with a 100 cycle fatigue increment at a peak load of 50% UTS is

shown in Figure 5b. Damage progression is seen to be highly discontinuous, with crack extension being dominated by the growth and coalescence of many small cracks, rather than the progression of a dominant crack tip. The primary process of damage propagation at the nominal crack tip, defined as the furthest extent of the damage zone, is represented by particle debonding (Figure 5b, (A)), which results in the creation of bridging ligaments along the crack wake. The process is distributed over a length of approximately 1 mm around the nominal crack tip, with partially debonded particles remaining intact relatively far behind the nominal crack tip (over several hundred micrometers) and acting as bridging ligaments between the crack flanks.

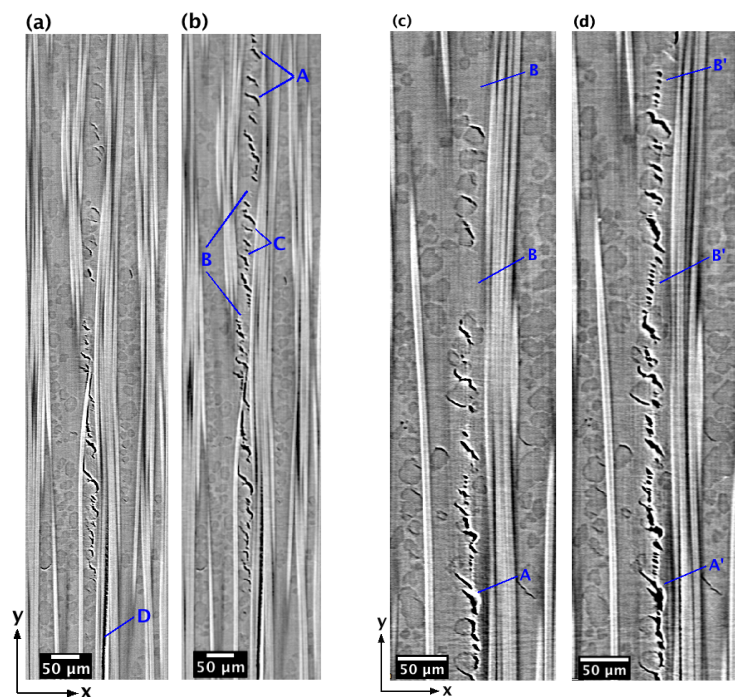


Figure 5 - 0° ply split growth propagation in the particle toughened system within the resin rich region for a peak load of 50% UTS: two comparisons at 700 cycles and 800 cycles (corresponding to (a)-(b) and (c)-(d)).

The periodicity and scale of microcracking is clearly defined by the particle size and separation distances, as shown in Figure 5b. Crack bridging ligaments consist of resin between particles debonds (e.g. Figure 5b, (B)) and/or particles themselves (e.g. Figure 5b, (C)). The presence of particles clearly promotes crack deflection, increasing the crack path tortuosity and the surface roughness. Figure 5a, (D) shows the difference between the split growth propagation along the fibre/matrix interface, which appears smooth/straight, versus the damage developed in the resin rich region, characterized by significant crack deflection. Considering another region of interest in

the coupon (Figure 5(c) and 5(d)), several bridging ligaments present at 700 cycles (Figure 5c (A) and (B)) are removed, wholly or partially, at 800 cycles (Figure 5d (A') and (B')). Two different behaviours have been detected, depending on the resin ligament size: (i) small bridges (on the order of $\sim 10\text{-}20\ \mu\text{m}$); these fail by connecting adjacent microcracks along the direction of damage propagation, as shown in Figure 5d (A'); and (ii) large ligaments (on the order of $\sim 50\text{-}100\ \mu\text{m}$ cross-section), fail by the formation of local echelon cracks within the bulk resin itself (i.e. not from toughening particles) at 45° to the loading direction, as shown in Figure 5d (B). Toughening particles act also as bridging ligaments when they are partially debonded along the crack wake, as shown in Figure 5d (C).

Single fibre breaks and doublets (two adjacent broken fibres) have been detected along the 0° ply split path associated with misaligned and bridging fibres. Further analyses conducted on tensile tests showed that the first cycle introduces just a few fibre breaks (~ 4) over the average crack length of $400\ \mu\text{m}$. The number of fibre breaks detected after 700 cycles is roughly fifteen times higher (56 fibre breaks) than in the quasi-static case, indicating that whilst fatigue loadings leads to additional fibre breaks.

4.2 Untoughened system

The untoughened system exhibits fewer and smaller resin-rich regions, especially within each individual ply. This microstructure clearly affects damage propagation, which occurs preferentially at the fibre/matrix interface (rather than at secondary phase particles in the toughened material) for both 0° ply splits and delaminations, as shown in Figure 6 for the specific case of a 0° ply split. As such, 0° ply splits manifest similar behaviour to the particle toughened system within the fibre packed regions, developing relatively straight and smooth fracture paths. This is depicted in Figure 6a and 6b, where damage (in cyan) was segmented to distinguish features with similar greyscale values.

When the fibres are surrounded by resin, the crack propagation was seen to be discontinuous, assuming the form of small microcracks at the fibre/matrix interface, retaining very small resin ligaments (on the order of a few micrometers), e.g. Figure 6c.

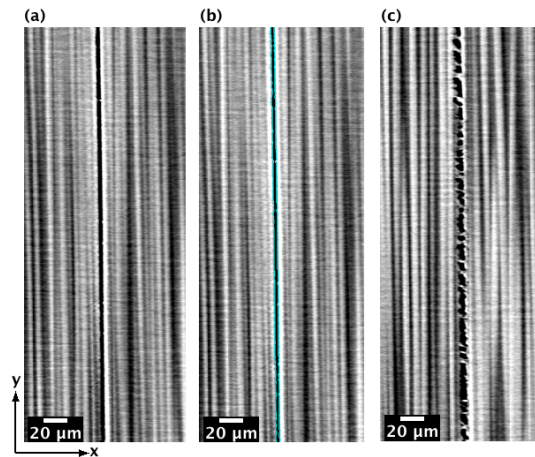


Figure 6 - 0° ply split propagation in the untoughened system: within the fibre packed region (a) with representation of the segmented damage (b), and in correspondence with fibres surrounded by resin (c). Peak load of 50% UTS and 700 cycles.

Fatigue loading of the untoughened system generated a higher number of fibre breaks for a given load level and number of cycles compared with the particle toughened system for which fibre breaks were observed only along the 0° ply split path. ~ 200 fibre breaks were counted for the untoughened material compared to the 56 detected for the particle-toughened system at the same stress and number of cycles. Specifically, the untoughened system shows single and multiple fibre breaks along the 0° ply split, but also a significant number of fibre breaks within the 0° plies, in the region between the 0° ply split paths. While it is clear that these are not all due to fibres bridging the splits, the mechanism of fibre failure away from the path of the split is unclear and merits further investigation.

4.3 Intrinsically toughened matrix system

The intrinsically toughened matrix (8552) resulted in fatigue micromechanical behaviour that is, in broad terms, intermediate to the untoughened and particle toughened systems. Intralaminar damage initiates in high fibre volume fraction regions as fibre debonding and propagates in a relatively straight/simple manner as detected for the untoughened system. Failure in the resin rich regions occurs via small microcracks originating at the fibre/matrix interface. The resin remaining between microcracks forms bridging ligaments, which are smaller than those in the particle-toughened system and of a similar scale to those observed in the untoughened system. Single and multiple fibre breaks have been detected along the 0° ply split paths and within the 0° plies in the regions close to the splits. No correlation with the presence

of delamination, as observed in the untoughened material, was found. For equivalent load conditions ~150 fibre breaks were detected for the intrinsically toughened material system in similar order to the untoughened system (191), *cf.* ~50 in the particle toughened material.

4.4 Crack morphology

Two-dimensional slices were exploited to segment fatigue damage and provide a 3D representation of the crack front profile, as shown in Figure 7. The investigation was focused on 0° ply splits with different crack profiles being detected, depending on the matrix system, and in particular on the interaction between damage and the local microstructure. The three-dimensional rendering of the damage within the particle-toughened system (Figure 7a) confirms that particles play a fundamental role in crack development. The local crack path is three-dimensional with a roughness and tortuosity defined by the particle size, with the crack and associated damage occupying a fraction of the intra-ply resin rich regions. By contrast, the untoughened material exhibits much more planar/uniform crack surfaces, with 3-D features largely determined by the scale of the fibre diameter and the inter-fibre spacing.

Figures 7a-c show plan views of splits from each material. Toughening mechanisms in the particle system are seen to act locally, within bands in the material, resulting in local fracture energy dissipation, consistent with the uneven crack advance, as shown in Figure 7a. The presence of retarded zones (pinning of the crack front) is related to the location of resin-rich regions containing the majority of toughening particles, which inhibit crack propagation, as shown in the cross-section perpendicular to the loading direction, Figure 7d. The result is a crack front that exhibits a “jagged” shape (Figure 7a), characterized by extended crack growth in the high fibre volume fraction regions, associated with extensive debonding of fibre/matrix interfaces. Figure 7b displays the 0° ply split segmentation for the untoughened system. Split propagation at the matrix/fibre interface is more uniform across the ply split width due to the absence of resin and particle-rich bands.

The crack propagation across the ply thickness is seen to occur on two distinct planes in this particular instance, corresponding to two different initiation sites, as shown in cross-section in Figure 7e. However, considering each branch separately the crack growth is relatively uniform, as shown in Figure 7b. Resin bridging ligaments (black regions within the segmentation) comprise a relatively small area fraction compared

with the particle-toughened material, with a corresponding expectation of reduced effectiveness of bridging and hence crack shielding.

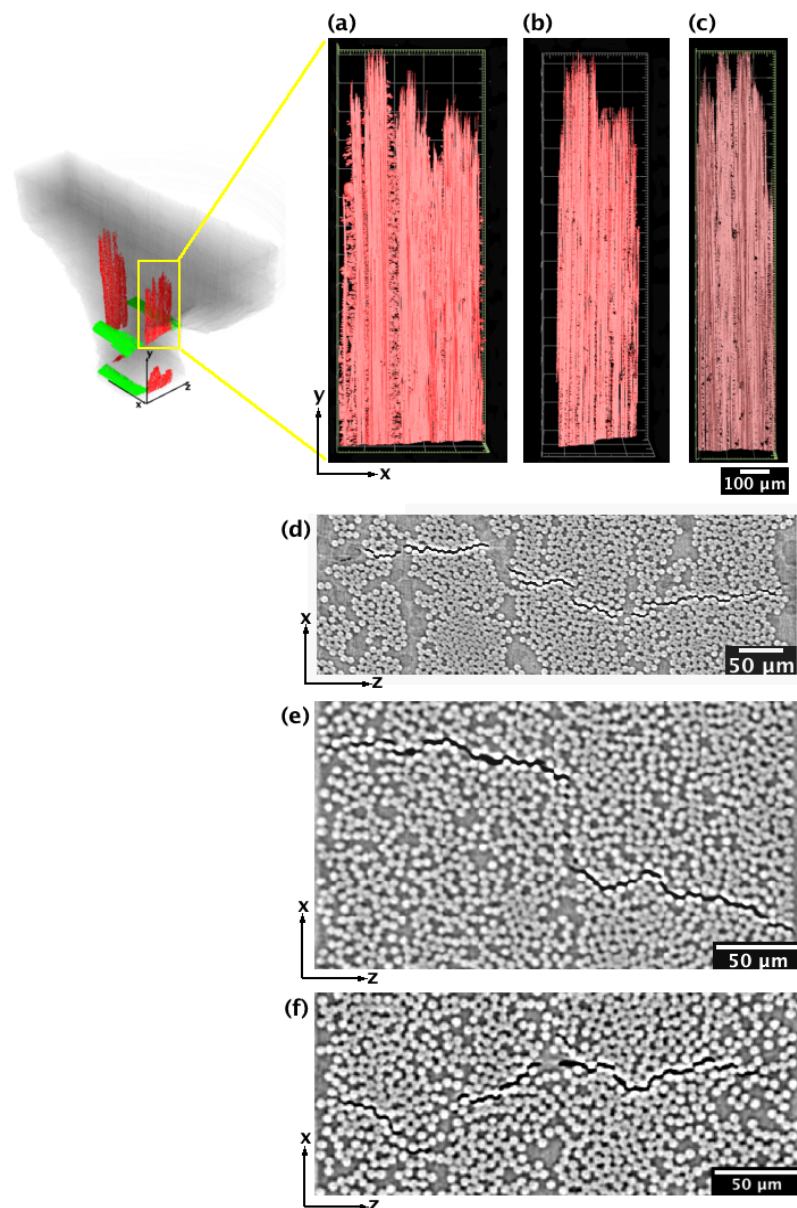


Figure 7 - Three-dimensional rendering of the 0° ply split, with a typical cross section perpendicular to the loading direction: (a), (d) particle-toughened system; (b), (e) untoughened system; and (c), (f) intrinsically toughened system. Peak load of 50% UTS and 800 cycles.

The intrinsically toughened system demonstrated an intermediate behaviour, between that of the particle-toughened and the untoughened systems, as shown in Figure 7c. In particular, even though no toughening particles are present within the matrix, the resin rich regions act as crack retardation sites, creating non-uniform crack growth. The cross-section perpendicular to the loading direction presented in Figure 7f confirms

that the split is constrained by a resin-pocket, whereas in fibre rich volumes crack growth is extended. The density of bridging ligaments along the crack wake is much less than for the particle-toughened system but is slightly higher than for the untoughened system.

The root mean square (RMS) “roughness” of the crack front profiles was calculated in order to quantify the variation. The particle toughened and the intrinsically toughened systems exhibited similar values (RMS $\sim 230 \mu\text{m}$), which were much higher than for the untoughened system (RMS $\sim 70 \mu\text{m}$).

5. Fatigue damage quantification

Damage quantification has been conducted focusing on the evaluation of the crack length and crack opening displacement of 0° ply splits, as shown in Figure 8. Three-dimensional damage rendering, shown in Figure 2, demonstrates that 0° ply splits are not planar; however, the COD map represents a 2D projection of the split onto the plane of the 0° plies, obtained by summing the voxels in the through-thickness direction. Figure 8(a) and Figure 8(b) show the crack opening contour map of 0° ply splits grown in fatigue loading at 30% and 50% UTS respectively for 10^4 cycles; where red corresponds to large values of COD, and blue regions are uncracked. The COD maps again show that the crack front growth does not advance evenly.

The COD map for an applied load of 30% UTS, Figure 8(a), exhibits two main regions across the split width (ply thickness) separated by a large resin rich region located roughly in the middle ($250 \mu\text{m}$), at the interface between the two central 0° plies. Both regions, from $50\text{--}220 \mu\text{m}$ and the other from $270\text{--}420 \mu\text{m}$, are characterized by a jagged crack front; with a similar overall extent on each side and retarded crack growth close to the interfaces with the 90° plies, i.e. from $0 \mu\text{m}$ to $50 \mu\text{m}$ and from $420 \mu\text{m}$ to $450 \mu\text{m}$, where the crack interacts with particles at the interfaces. Another prominent resin rich region is located between $180\text{--}200 \mu\text{m}$. The COD values appear similar across the majority of the split, with average values on the order of $2.5\text{--}3.5 \mu\text{m}$ at the root and $1.5\text{--}2.5 \mu\text{m}$ in the region $200 \mu\text{m}$ back from the crack tip. The COD map obtained for an applied load of 50% σ_f is shown in Figure 8(b). Similar behaviour at the lower load is observed: two main zones are visible across the split width (ply thickness), from $50 \mu\text{m}$ to $250 \mu\text{m}$ and from $270 \mu\text{m}$ to 500

μm , corresponding to regions of higher fibre volume fraction, and separated by a resin rich region in the middle of the ply, at $250 \mu\text{m}$. The split shape is similar to the lower load case, with a comparable local jagged region of amplitude $200\text{-}250 \mu\text{m}$. The increase in load clearly results in a longer crack length for the same number of cycles (10^4), higher COD at the root, and reduced bridging within the resin rich regions and at the interfaces.

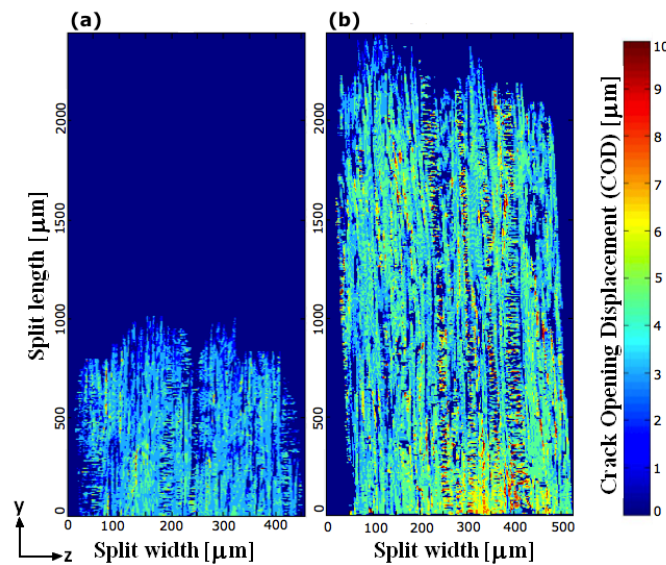


Figure 8 - Fatigue crack opening displacement mapping for 0° ply splits at: (a) 30% UTS and (b) and 50% UTS (10^4 cycles).

Higher local values of COD have been also detected; mostly located along the cracked resin rich regions (e.g. $250\text{-}270 \mu\text{m}$ and $400\text{-}420 \mu\text{m}$), within which the “echelons” of microcracks oriented at 45° with respect to the loading direction are clearly visible along the split length. The average COD values decrease from the root towards the crack tip. The COD map in Figure 8(b) depicts values in the order of $4.5\text{-}6 \mu\text{m}$ close to the root (within $250 \mu\text{m}$) and in the range of $3\text{-}4.5 \mu\text{m}$ for the majority of the crack length. The crack opening displacement at the same distance ($\sim 250 \mu\text{m}$) back from the notch tip is similar to that measured for the lower load; within the range of $1.5\text{-}3 \mu\text{m}$. It should be noted that the minimum COD value measurable is associated with the voxel resolution, which in this case is $1.5 \mu\text{m}$ (crack tip locations may still be located at openings less than the voxel size however due partial volume effects). Locations along the 0° ply splits have been referenced with respect to distance from the crack tip, in order to compare the COD evolution associated with

these two different split lengths. For instance, at a position of 500 μm back from the crack tip for both loading conditions, the COD is lower for the lower load case. This is in part simply attributable to the load difference, but it is also clear that there has been additional degradation of crack wake bridging ligaments at the higher loading. In particular at the central ply interfaces, close to the crack tip, there is a smaller intact bridging region at the higher load case (8(b)) compared to that present in the lower load case (8(a)).

6. Fatigue and quasi-static damage comparison

Qualitative analyses via 3D rendering of damage demonstrate broadly similar behaviour between fatigue and quasi-static loading [15] in terms of crack location and shape. However, fatigue loading results in more extensive damage than for quasi-static loading at the same peak load. In addition, delamination is *not* detected under quasi-static loading for these load levels, whereas delamination is clearly observed in the fatigue case. In both quasi-static and fatigue a similar correlation between intralaminar damage and microstructure was observed, suggesting broadly similar micromechanical behaviour of 0° ply split propagation in resin rich regions and high-fibre volume fraction regions. Figure 9 displays a cross section of a 0° ply split in a resin rich-region for quasi-static loading (Figure 9(a)), and for fatigue (Figure 9(b)); both cases loaded at 50% UTS.

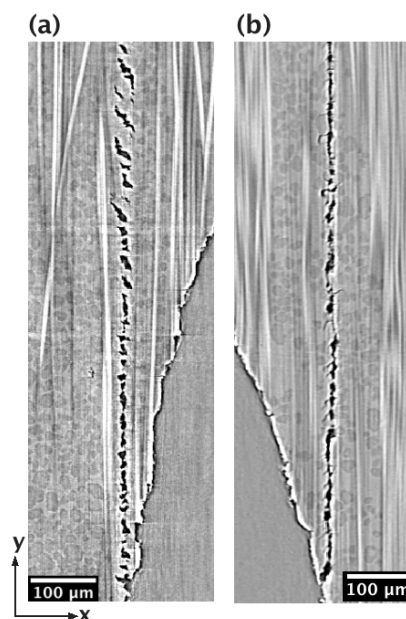


Figure 9 - Comparison of the micromechanical behaviour along the 0° ply split in (a) quasi-static case loaded to 60% UTS, and (b) fatigue loaded to 50% UTS with number of cycles of 10^4 .

The discrete microcracks in the resin rich regions are much more apparent in the quasi-static loading case, as shown in Figure 9(a). In cyclic loading the bridges between the individual microcracks appear to have largely failed, presumably due to local cyclic degradation, yielding more continuous cracks as shown in Figure 9(b).

In order to provide a direct comparison of crack morphology between the fatigue and quasi-static loading, CODs have been compared between 0° ply splits of two similar total lengths (1mm and 2.5mm) obtained in fatigue (albeit at lower maximum load levels) and quasi-static loading as shown in Figure 10. Fatigue plots correspond to the cases with peak loads of 30% and 50% UTS, and 10^4 cycles; whereas the quasi-static cases were obtained at load levels of 70% and 60% UTS respectively. Both fatigue and quasi-static loading result in similar features: a jagged crack front, with greater crack advance along areas with higher local fibre volume fractions, and crack retardation along resin rich regions with the formation of bridging ligaments and echelons of microcracks oriented at 45° with respect to the loading direction in the resin rich regions.

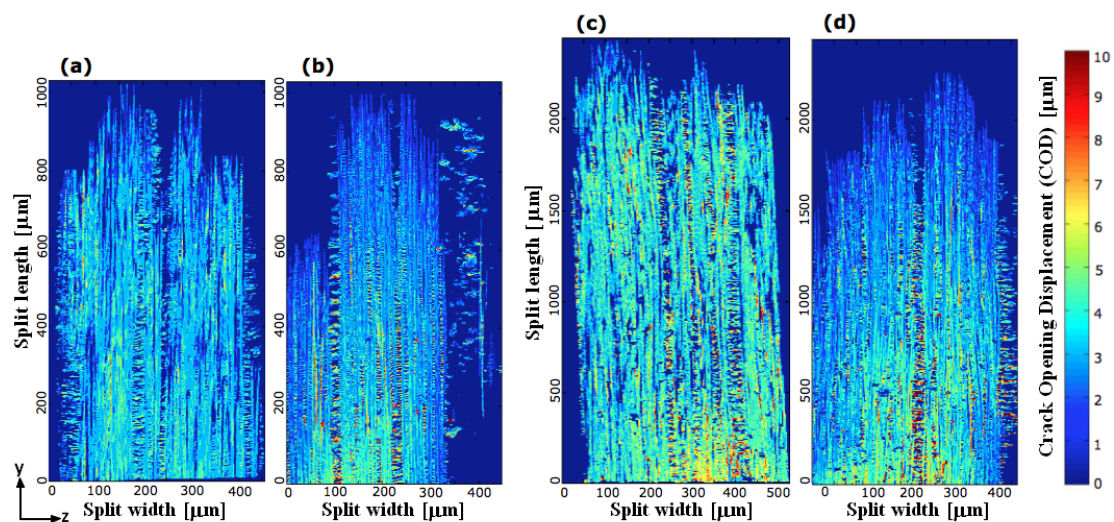


Figure 10 - Split crack opening displacement contours: (a) crack length of 1 mm: fatigue case with peak load of 30% UTS and 10^4 cycles, (b) quasi-static case for 70% UTS; crack length of 2.5 mm: (c) fatigue case with peak load of 50% UTS and 10^4 cycles, and (d) quasi-static case for the load of 60% UTS.

The fatigue-loaded specimens show more uniform crack advance across the ply thickness, along with more uniform crack opening displacement over the area of the crack (width and length). In terms of uniformity of crack length across the ply thickness (split width), large uncracked resin rich areas characteristically seen in static load cases (e.g. a band of $\sim 100\mu\text{m}$ width along the right hand ply interface of the 0°

ply split in Figure 10(b)) were largely absent in the fatigue loading cases. Comparing Figure 10(a) with 10(b) and Figure 10(c) with 10(d), it is apparent that in the quasi-static cases (10b, 10d) there is a significantly higher crack opening displacement towards the centre line of the 0° ply split and/or the centre line of the resin rich regions. Figures 10(a) and 10(c), associated with fatigue loading, show more uniform crack opening displacements across the ply thickness. The comparison between these two loading conditions highlights the presence of higher average values of COD in the fatigue cases (Figure 10a, 10c), even though the applied loads were higher for the quasi-static cases (Figure 10b, 10d). In the first instance, this is consistent with a reduced number and strength of load bearing ligaments in the wake of the fatigue cracks, and/or the corresponding incidence of delamination in fatigue. The presence of delamination in the fatigue case could affect the COD due to the fact that the 0° plies are less constrained. However, the delamination is not completely developed along the split length, as shown in Figure 2, extending only along 10% and 35% of the total 0° ply split lengths considered for the COD maps for the cases of loading at 30% and 50% σ_f respectively. Quasi-static cases showed no delamination for the smaller crack and minimal of delamination for the longer crack (amounting to $\sim 5\%$ of the 0° ply split length). As such, higher CODs for the fatigue cases compared to similar split lengths in quasi-statically loaded specimens are consistent with the local degradation of bridging ligaments under fatigue loading, as illustrated in Figure 10(a) and 10(c), resulting in reduced effectiveness of bridging and higher crack opening and shear displacements.

7. Conclusions

SRCT combined with *in situ* loading has been demonstrated as an effective technique for investigating the micromechanisms of fatigue in composite materials with toughened matrices. Several novel observations have been obtained for the micromechanisms of fatigue crack growth.

Broadly similar micromechanisms of damage initiation have been identified in fatigue and quasi-static loading in a particle-toughened carbon fibre-epoxy composite system. Cracks nucleate in the matrix/fibre-matrix interface region within volumes of high local fibre-volume fraction within the 0° plies. This initial stage is not characterized by the propagation of a single dominant crack, but multiple microcracks separated by

bridging ligaments. As such, the micromechanisms of damage initiation are similar to those of damage propagation. Results showed that damage propagation is closely related to the local microstructure. Toughened systems exhibit different damage behaviour in resin-rich regions and fibre-packed zones, which appears to exaggerate non-uniform crack growth. Zones of retarded crack growth correspond to resin rich regions, which contain bridging ligaments. This was most pronounced in the particle-toughened system, and less so in the intrinsically-toughened system. There is evidence that the load cycling contributes to progressive failure of bridging ligaments in the crack wake, especially in the toughened particle system. The untoughened system showed more uniform damage propagation across the crack front, due to the more uniform microstructure. Consequently, fracture occurs by the propagation of a well-defined crack front, whereas in the toughened systems there is extensive micro-cracking ahead of the crack tip and crack bridging processes behind the crack tip. The untoughened system showed a higher number of fibre breaks within the 0° plies with respect to the toughened systems, particularly within regions close to the 0° ply splits. It seems likely that a key mechanism of fatigue in the toughened-particle system on intralaminar loading is the degradation of bridging ligaments introduced by particles in the fatigue crack wake rather than due to processes at, or ahead of the crack tip; resulting in higher, more uniform crack opening displacements and less-serrated crack fronts compared to quasi-static loading.

8. Significant Contributions

This study has made the following original contributions:

1. First use of synchrotron radiation computed tomography to investigate the micromechanisms of fatigue in fibre composite materials, identifying 3D crack behaviour down to ~300nm resolutions.
2. First comparison of micromechanisms of fatigue between toughened and untoughened systems.
3. First identification of the role of bridging ligaments in generating damage resistance (toughness) in all materials investigated via quantitative mapping of local crack opening displacements
4. First identification of the effect of fatigue on failure of crack bridging ligaments.

5. First quantification of the effect of fatigue on fibre failure, particularly identifying systematic differences between toughened and untoughened systems.

9. Future Work

The study has made significant contributions to our understanding of the effects of fatigue in fibre-reinforced composite materials. It has identified several important areas for follow-on research:

1. The ability to quantify damage at high resolution allows for the possibility of the application of data rich mechanics techniques to model the processes and provide guidance for design and material improvement. In a separate project the augmented finite element method (AFEM) is being applied to understand the progression of cracks through particle-toughened interlayers. This work could be extended to include the effect of fatigue loading.
2. The work carried out herein has necessarily been conducted on small-scale specimens. A key piece of follow-on work is to link the results to macro-scale coupons and in service test articles, to ensure that similar mechanisms are observed. There is also the possibility to link to NDE and Structural Health Monitoring techniques to provide validation.
3. The observations of fibre fracture in fatigue are of great significance. They are quite different from observations previously made in quasi-static loading. Understanding the fibre failure is a key to understanding tensile strength, and has the potential to improve fibre-utilisation and the structural efficiency of composite parts. There are also long standing questions about very long term strength reduction in composite parts held under load.

Acknowledgments

The authors would like to acknowledge funding from AFOSR-EOARD, grant 113040, Programme Monitor: Lt. Col. Randall Pollak. Also funding from EPSRC, grant EP/H1506X/1. The authors are grateful to the Swiss Light Synchrotron Radiation for access to TOMCAT-X02DA beamline, and to the assistance of Dr. Bernd Pinzer, Dr. Sarah Irvine, and Dr. Peter Modregger. Thanks to μ -VIS at the University of

Southampton for the computer analysis facilities. Materials were supplied via Airbus SAS and Teledyne Technologies Incorporated.

References

- [1] C. Soutis “Fibre reinforced composites in aircraft construction”. *Progress in Aerospace Science*, Vol. 41, No. 7, pp. 143-151, 2005.
- [2] S.M. Spearing and P.W.R. Beaumont “Fatigue damage mechanics of composite materials. I: Experimental measurement of damage and post-fatigue properties”. *Composites Science and Technology*, Vol. 44, No. 2, pp. 159-168, 1992.
- [3] C. Koimtzoglou, V. Kostopoulos and C. Galiotis “Micromechanics of reinforcement and damage initiation in carbon fibre/epoxy composites under fatigue loading”. *Composites Part A: Applied Science and Manufacturing*, Vol. 32, No. 3-4, pp. 457-471, 2001.
- [4] J.R. Gregory and S.M. Spearing “Constituent and composite quasi-static and fatigue fracture experiments”. *Composites Part A: Applied Science and Manufacturing*, Vol. 36, No. 5, pp. 665-674, 2005.
- [5] O.J. Nixon-Pearson, S.R. Hallett, P.J. Withers, J. Rouse. “Damage development in open-hole composite specimens in fatigue. Part I: Experimental investigation”. *Composite Structures*, Vol. 106, pp. 882-889, 2013.
- [6] Y.A. Dzenis “Cycle-based analysis of damage and failure in advanced composite under fatigue 1. Experimental observation of damage development within loading cycles”. *International Journal of Fatigue*, Vol. 25, No. 6, pp. 499-510, 2003.
- [7] S.M. Spearing, P.W.R. Beaumont and M.F. Ashby “Fatigue damage mechanics of composite materials. II: a damage growth model”. *Composites Science and Technology*, Vol. 44, No. 2, pp. 169-177, 1992.
- [8] O.J. Nixon-Pearson, S.R. Hallett, P.W. Harper, L.F. Kawashita “Damage development in open-hole composite specimens in fatigue. Part 2: Numerical modelling”. *Composite Structures*, Vol. 106, pp. 890-898, 2013.
- [9] M. Beghini, L. Bertini and E. Vitale “Analysis of fatigue delamination growth in carbon fibre specimen with central hole”. *Composite Structures*, Vol. 17, No. 3, pp. 257-274, 1991.
- [10] A.P. Mouritz, C. Townsend and M.Z. Shah Khan “Non-destructive detection of fatigue damage in thick composites by pulse-echo ultrasonics”. *Composites Science and Technology*, Vol. 60, No. 1, pp. 23-32, 2000.
- [11] Y.A. Dzenis “Cycle-based analysis of damage and failure in advanced composite under fatigue 1. Experimental observation of damage development within loading cycles”. *International Journal of Fatigue*, Vol. 25, No. 6, pp. 499-510, 2003.
- [12] S. Blassiau, A.R. Bunsell and A. Thionnet “Damage accumulation processes and life prediction in unidirectional composites”. *Proceeding of the Royal Society A*, Vol. 463, No. 2080, pp. 1135-1152, 2007.
- [13] L. Toubal, M. Karama and B. Lorrain “Damage evolution and infrared thermography in woven composites laminates under fatigue loading”. *International Journal of Fatigue*, Vol. 28, No. 12, pp. 1867-1872, 2006.
- [14] E. Maire, P.J. Withers “Quantitative X-ray tomography”. *International Materials Review*, Vol. 59, No. 1, pp. 1-43, 2014.
- [15] A.E. Scott, M. Mavrogordato, P. Wright, I. Sinclair and S.M. Spearing “In situ fibre fracture measurement in carbon-epoxy laminates using high resolution computed tomography”. *Composites Science and Technology*, Vol. 71, No. 12, pp. 1471-1477, 2011.
- [16] P. Wright, A. Moffat, I. Sinclair and S.M. Spearing “High resolution tomographic imaging and modeling of notch tip damage in laminated composite”. *Composites Science and Technology*, Vol. 70, No. 10, pp. 1444-1452, 2010.
- [17] A.J. Moffat, P. Wright, J.-Y. Buffiere, I. Sinclair and S.M. Spearing “Micromechanisms of damage in 0° splits in a [90/0]_s composite material using synchrotron radiation computed tomography”. *Scripta Materialia*, Vol. 59, No. 10, pp. 1043-1046, 2008.
- [18] D.J. Bull, S.M. Spearing, I. Sinclair, L. Helfen “Three-dimensional assessment of low velocity impact damage in particle toughened composite laminates using micro-focus X-ray computed

- tomography and synchrotron radiation laminography”. *Composites: Part A*, Vol. 52, pp. 62-69, 2013.
- [19] Hexcel HexPly M21. http://www.hexcel.com/Resources/DataSheets/Prepreg-Data-Sheets/M21_global.pdf.
- [20] Hexcel HexPly 8552. http://www.hexcel.com/Resources/DataSheets/Prepreg-Data-Sheets/8552_eu.pdf
- [21] 3501-6 Epoxy Matrix, Hexcel. http://www.hexcel.com/Resources/DataSheets/Prepreg-Data-Sheets/3501-6_eu.pdf
- [22] B.A. Dowd, G.H. Campbell, R.B. Marr, V. Nagarkar, S. Tipnis, L. Axe and D.P. Siddons “Developments in synchrotron x-ray computed tomography at the National Synchrotron Light Source”. *Proc. SPIE* 3372, pp. 224-236, 1999.
- [23] S.C. Garcea, M.N. Mavrogordato, A.E. Scott, I. Sinclair, S.M. Spearing “Fatigue micromechanism characterisation in carbon fibre reinforced polymers using synchrotron radiation computed tomography”. *Composites Science and Technology*, Vol. 99, pp. 23-30, 2014.